JOURNAL OF AIRCRAFT
Vol. 33, No. 5, September–October 1996

NPARC Study of a Two-Dimensional Transonic Wall Interference

M. Khalid* and M. Mokry†
National Research Council, Ottawa, Ontario K1A 0R6, Canada

An application of the inviscid (Euler) version of the NPARC code to a finite thickness airfoil inside a test section with impermeable walls is described. Three different, physically meaningful, choking patterns are generated. It is shown that, in contrast to predictions from singular perturbation analyses, the computed wind-tunnel results are not correctable to equivalent freestream conditions when flow is choked.

Nomenclature

A = cross-sectional area
C_p = pressure coefficient
C_L^u = upper-surface lift coefficient
c = chord length of airfoil
h = height of test section
M = local Mach number
M_{ch} = choking Mach number
$M_{ch}^{(1)}$ = choking Mach number, subsonic
$M_{ch}^{(2)}$ = choking Mach number, supersonic
M_T = wind-tunnel Mach number
M_∞ = Mach number imposed on outer boundary
t = maximum thickness of airfoil
x = chordwise coordinate
γ = ratio of specific heats

I. Introduction

THE subject of transonic wind-tunnel wall interference, despite extensive research in the last half-century, is still insufficiently documented to enable a formulation of readily applicable correction procedures. The conclusions from the application of transonic similarity rules[1] and singular perturbation methods[2–4] are essentially that for a thin airfoil there exists a correction to the stream velocity that accounts adequately for the effect of the distant wind-tunnel walls. These studies are of fundamental importance in showing that the wall interference corrections for the near-sonic conditions at the walls, being subject to transonic rather than subsonic scaling, are finite. The most serious limitation of the transonic singular-perturbation theory is that it only describes what happens in the limit of an infinitely thin airfoil in a very large wind tunnel at sonic-flow conditions. Extensions of the theoretical thin-airfoil results to an arbitrary thick airfoil in a finite size wind tunnel are difficult to substantiate experimentally, because small variations of flow quantities need to be measured in a regime for which the wind tunnels are most difficult to calibrate.

The currently available computational fluid dynamic (CFD) techniques, such as the Euler or Navier–Stokes NPARC codes,[5] are far more flexible in this regard and permit numerical simulation of the effect of wind-tunnel walls on a model throughout the entire transonic speed range. However, special attention must be paid to the imposition of appropriate boundary conditions, both along the walls and at the entrance and exit boundaries of the test section. These conditions are expected to describe flow in the vicinity of an actual wind-tunnel wall as realistically as possible and also comply with the conservation laws. Another sensitive point, as we shall see later, is interpretation of the CFD result in terms of actual wind-tunnel flow.

This article describes numerical experimentation with the inviscid (Euler) version of the NPARC code, applied to an airfoil in free-air and inside a test section with closed (impermeable) walls. The corresponding Slip-Surface condition, already built in the code, is much easier to impose than, for example, the boundary conditions for ventilated walls. However, because choking in this case is not alleviated by transpiration, it also represents the most severe test case as far as transonic wall interference is concerned. The free-air calculations serve as comparisons on the basis of which the questions of correctability of wind-tunnel results are discussed.

II. Boundary Conditions

The boundary conditions (and their identifiers) used with the two-dimensional, inviscid-flow version of the NPARC code are

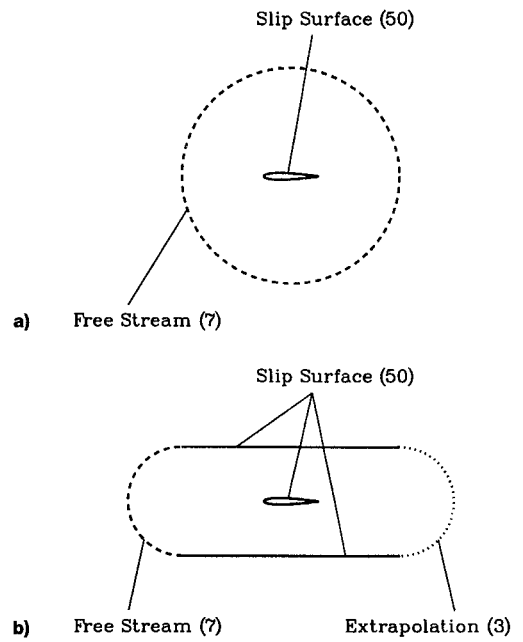

Fig. 1 Boundary conditions for free-air and wind-tunnel domain: a) free-air and b) wind tunnel.

Received Nov. 28, 1995; presented as Paper 96-0496 at the AIAA 34th Aerospace Sciences Meeting and Exhibit, Reno, NV, Jan. 15–18, 1996; revision received May 7, 1996; accepted for publication May 7, 1996.

*Senior Research Officer, Aerodynamics Laboratory, Institute of Aerospace Research. Member AIAA.

†Senior Research Officer, Aerodynamics Laboratory, Institute of Aerospace Research. Senior Member AIAA.

shown schematically in Fig. 1. The Free Stream condition was imposed both as an external far-field boundary condition for the free-air solution and as the upstream boundary condition for the wind-tunnel solution. The Extrapolation boundary condition, which equates the flow variables at the boundary to their values one grid point upstream, was selected at the downstream end of the wind-tunnel grid domain. It was found to perform reasonably well for both subsonic and supersonic velocities of the stream. The Free Stream condition was also tried as a downstream boundary condition, but performed satisfactorily only at subcritical flow conditions, when flow was isentropic. The Slip-Surface boundary condition, in which all flow gradients normal to this surface along with the normal component of velocity are set equal to zero, was used both on the airfoil and the wind-tunnel walls.

III. Mesh

A single-block wind-tunnel mesh was developed by compressing an O-mesh around the airfoil to fill the computational domain. As already indicated in Fig. 1b, the wind-tunnel walls were represented by two parallel lines. To preserve the slope isotropy of the mesh the upstream and downstream ends were shaped as half-circles.

An example of the central portions of 161 × 33 O-meshes for a NACA 0012 airfoil is shown in Fig. 2. To facilitate a meaningful comparison[6] of wind-tunnel and free-air solutions, the inner 16 layers of the meshes were kept identical. The outer 16 layers of the wind-tunnel mesh were compressed to fill the wind-tunnel domain by redistributing the grid points in the radial direction as a geometric sequence. The test section height is 5 chord lengths and the walls extend 10 chord lengths both upstream and downstream. The mesh lines inside the blanked-out invariant region are in enlarged scale seen in Fig. 3.

As may be observed in Figs. 2 and 3, the mesh is orthogonal at the airfoil, but not at the wind-tunnel walls or the inflow and outflow boundaries. However, the skewness of the mesh at the outer boundaries has not been found to be a source of major numerical inaccuracies when compared with similar computations on a boundary-orthogonal, five-block mesh by Hawken.[7]

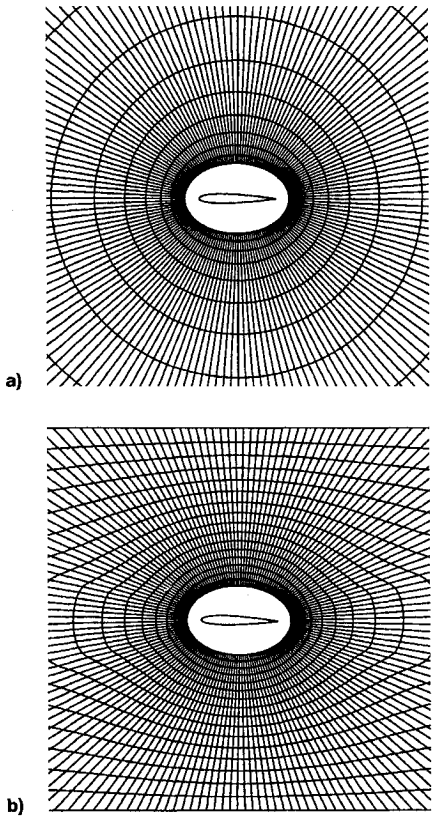

Fig. 2 Central portion of the 161 × 33 mesh: a) free-air and b) wind tunnel.

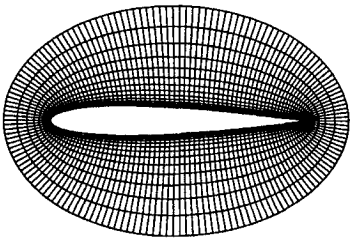

Fig. 3 Invariant portion of the 161 × 33 mesh.

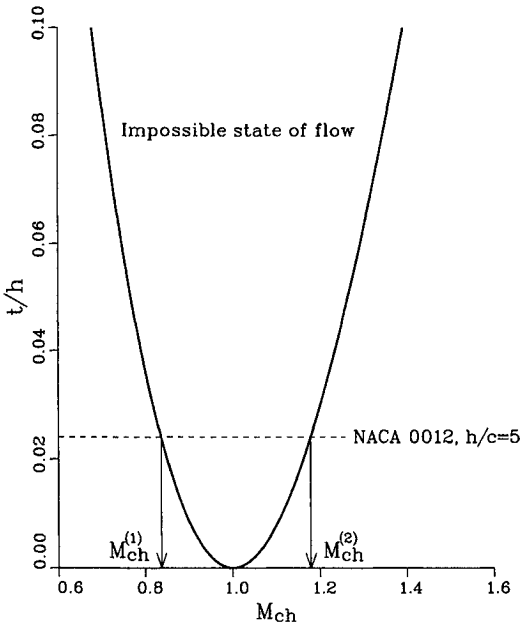

Fig. 4 Choking Mach number in one-dimensional flow.

IV. Choking Interval

As mentioned in Sec. I, with the NPARC code it is possible to perform computations covering the entire range of the transonic Mach number M_∞ imposed at the upstream end of the wind-tunnel flow domain. In analyzing the computational result, an important factor restricting the range of meaningful physical solutions is the phenomenon of choking. Assuming one-dimensional isentropic flow, the Mach numbers at cross sections A_1 and A_2 of a stream tube relate according to

$$\frac{A_2}{A_1} = \frac{M_1}{M_2}\left[\frac{2 + (\gamma - 1)M_2^2}{2 + (\gamma - 1)M_1^2}\right]^{(\gamma+1)/2(\gamma-1)}$$

Putting $A_1 = h$, $A_2 = h - t$, and $M_2 = 1$, we obtain the choking Mach number $M_1 = M_{ch}$, implicitly as a function of the maximum thickness-to-test section height ratio[8]:

$$\frac{t}{h} = 1 - M_{ch}\left[1 + \frac{\gamma - 1}{\gamma + 1}(M_{ch}^2 - 1)\right]^{-[(\gamma+1)/2(\gamma-1)]} \tag{1}$$

The dependence for $\gamma = 1.4$ is a 6th-order parabola with the vertex at $t/h = 0$ and $M_{ch} = 1$ (see Fig. 4). For a given $0 < t/h < 1$, Eq. (1) has two roots, $1 > M_{ch}^{(1)} > 0$ and $1 < M_{ch}^{(2)} < \infty$, determining the subsonic and supersonic limits of the choking interval, respectively. The choking interval $M_{ch}^{(1)} < M_1 < M_{ch}^{(2)}$

represents an impossible state of flow,[8] but interesting situations arise at its endpoints. If the upstream Mach number is equal to $M_{ch}^{(1)}$, the downstream Mach number is either $M_{ch}^{(1)}$ or $M_{ch}^{(2)}$. Similarly, if the upstream Mach number is $M_{ch}^{(2)}$, the downstream Mach number is again either $M_{ch}^{(2)}$ or $M_{ch}^{(1)}$. For one-dimensional isentropic flow there is a total of four possibilities.

For a 12% thick NACA 0012 profile and a wind tunnel of height-to-airfoil chord ratio of 5, the blockage ratio is $t/h = 0.024$, and we obtain $M_{ch}^{(1)} = 0.837$ and $M_{ch}^{(2)} = 1.179$. The actual choking Mach numbers will slightly differ because, in contrast to the one-dimensional case, the sonic line is neither normal to flow nor starts at the point of maximum airfoil thickness. This may be verified in Fig. 5, which shows three out of four possible choking patterns obtained by the NPARC code. In these patterns, which will be discussed in more detail later, the sonic line emanating on the forward part of the airfoil is indicated by a broken line. The one-dimensional estimates of $M_{ch}^{(1)}$ and $M_{ch}^{(2)}$ provide a convenient reference and may be used to mark the approximate limits of the choking interval in charts. However, when referring to $M_{ch}^{(1)}$ or $M_{ch}^{(2)}$ in text, we shall have the actual (exactly not obtainable) values in mind.

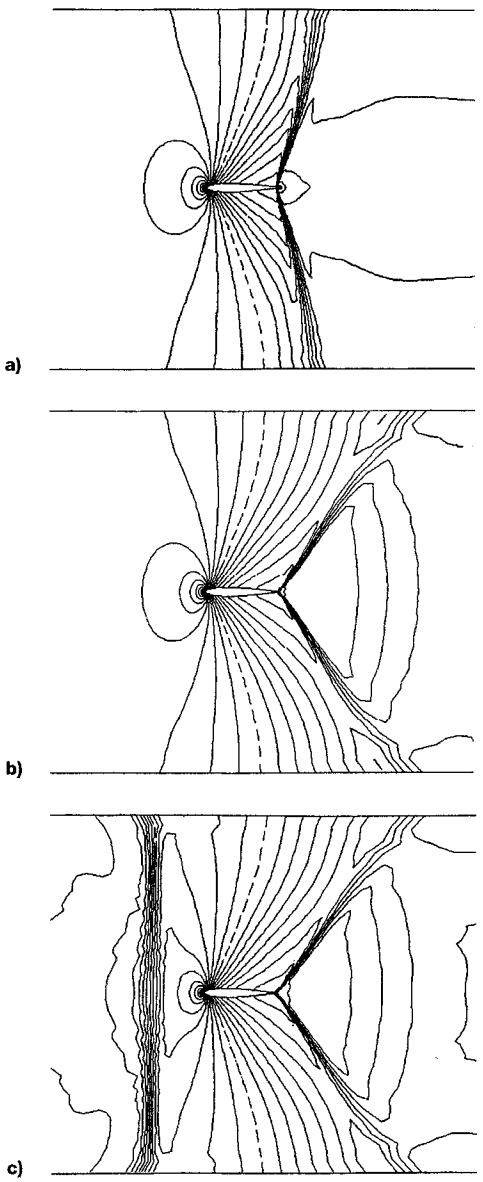

Fig. 5 Choked-flow isomachs for a NACA 0012 in wind tunnel (h/c = 5): a) subsonic–supersonic–subsonic, b) subsonic–supersonic, and c) supersonic–subsonic–supersonic.

V. Results and Discussion

The key computational results obtained for a NACA 0012 at zero incidence and the wind-tunnel height-to-airfoil chord ratio of 5 are displayed in Fig. 6. The upper-surface lift coefficient

$$C_L^u = -\frac{1}{c}\int_{-c/2}^{c/2} C_p \, dx \tag{2}$$

computed for the airfoil in the wind tunnel is compared there with that computed in the free-air flow for the same value of M_∞. We observe that for $M_\infty \leq M_{ch}^{(1)}$ the value of C_L^u in the wind tunnel is higher than that in free air. The corresponding Mach number correction is positive, because for a given C_L^u on the wind-tunnel curve we have to move in the direction of the increasing M_∞ to reach the corresponding value of C_L^u on the free-air curve. (The free-air value of C_L^u is slightly less since it has to be adjusted for a positive Mach number increment.) Similar conclusions can also be drawn from Fig. 7, where the shock-wave locations on the profile in free-air and wind tunnel are plotted. The sign and magnitude of the correction are consistent with experimental observations of blockage interference in closed-wall test sections. The actual wind-tunnel experiments, for the most part, are assumed to be correctable: in the subsonic speed range by linear superposition

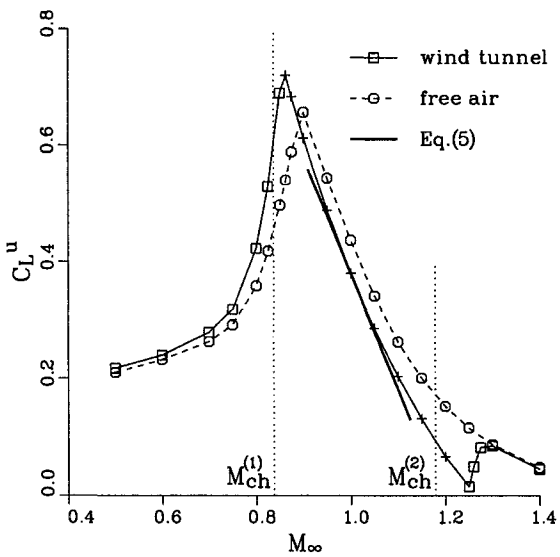

Fig. 6 Upper-surface lift coefficient for a NACA 0012 in free-air and wind tunnel (h/c = 5).

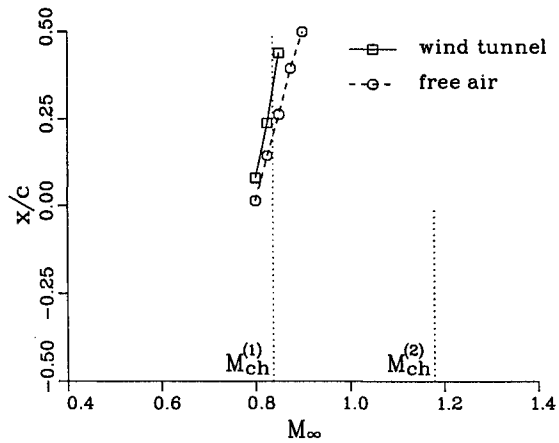

Fig. 7 Shock-wave location for a NACA 0012 in free-air and wind tunnel (h/c = 5).

methods and in the lower transonic range by some more recently developed nonlinear techniques.[9]

Having taken into consideration the choked-flow limits outlined in Fig. 4, it was first a little surprising to observe that the computation went through smoothly (about 2000 iterations) for any prescribed $M_{ch}^{(1)} \leq M_\infty \leq M_{ch}^{(2)}$. The computed C_L^u over the choking interval decreases monotonically with increasing M_∞, similarly to that evaluated in free-air, see Fig. 6. The explanation for not having encountered convergence difficulties can be found in the design of the mesh. Similarly to a decompression ahead of a converging–diverging diffuser in free-air,[10] flow upstream of the walls is given the chance to decelerate to a velocity compatible with the internal mass-flux constraint. The computational scheme behaves very much like an actual wind tunnel, overriding a Mach number setting that is not physically possible. This is illustrated in Fig. 8, where M_T, calculated 8 chord lengths ahead and aft of the airfoil, as functions of M_∞ are plotted. The upstream M_T (solid symbols) equals M_∞, but only outside the choking interval. Inside, the upstream M_T remains frozen at $M_{ch}^{(1)}$, while the downstream M_T (open symbols) jumps to $M_{ch}^{(2)}$ and stays frozen at this higher supersonic level. Eventually, at the upper end of the choking interval the upstream M_T undergoes a jump from $M_{ch}^{(1)}$ to $M_{ch}^{(2)}$ and from then on follows M_∞. The value of M_T downstream is less than that upstream because the process is not isentropic.

To trace the streamwise variations inside the wind tunnel, we have also plotted in Fig. 9 the local Mach number calculated along the walls, as a function of the normalized axial distance. At low subsonic speeds we observe a fairly uniform Mach number distribution, disturbed only on the portions of the walls immediately opposite the airfoil. The doublet-type disturbance[11] generated by the airfoil grows in magnitude as the stream Mach number increases.

A qualitative change occurs once the wall signature crosses $M = 1$, which also signals the onset of choking. The mass flux has reached its maximum value and the upstream tunnel Mach number can no longer increase. As has already been discussed, the inlet portion of the mesh sees M decrease from the prescribed value of M_∞ to $M_{ch}^{(1)}$, which is dictated by the internal mass flux constraint. At about 8 chord lengths upstream, used as the reference distance to define M_T in Fig. 8, all Mach number curves generated in the interval $M_{ch}^{(1)} \leq M_\infty \leq M_{ch}^{(2)}$ coalesce to $M_{ch}^{(1)}$.

It is also worth noting that of the computed choked-flow signatures in Fig. 9, only the first one ($M_\infty = 0.85$) turned subsonic after crossing $M = 1$. We shall denote this case as $M_{ch}^{(1)} \rightarrow M_{ch}^{(1)}$. All other signatures ($M_\infty > 0.85$) became supersonic downstream of the airfoil, establishing a second plateau $M_{ch}^{(2)}$ at about 8 chord lengths downstream. These signatures, which no longer have the appearance of a subsonic doublet disturbance, characterize the case $M_{ch}^{(1)} \rightarrow M_{ch}^{(2)}$.

The broken lines in Fig. 9 are the signatures obtained for $M_\infty \geq M_{ch}^{(2)}$. The combined effect of the nose and tail shock waves lends them an appearance of N-waves. In particular, the signature that is closest to choking is seen to dip down upstream of the airfoil and join that corresponding to the case $M_{ch}^{(1)} \rightarrow M_{ch}^{(2)}$. From Fig. 8 it is apparent that choked flow $M_{ch}^{(2)} \rightarrow M_{ch}^{(2)}$, similarly to $M_{ch}^{(1)} \rightarrow M_{ch}^{(1)}$, is an isolated case that is difficult to capture exactly. From the same figure it is also seen that choked flow $M_{ch}^{(2)} \rightarrow M_{ch}^{(1)}$ is nonexistent, or at least very unlikely.

The isomachs (contour interval 0.05) of the three observed choked flows are shown in Fig. 5. The flow patterns $M_{ch}^{(1)} \rightarrow M_{ch}^{(1)}$ and $M_{ch}^{(1)} \rightarrow M_{ch}^{(2)}$, shown in Figs. 5a and 5b, are identical upstream of the dashed sonic line. Physically, this is consistent with the fact that upstream traveling disturbances cannot cross this line, and flow upstream is thus isolated from further development downstream. The main difference in the two observed flow patterns is in the tail shock wave, which terminates the supersonic expansion over the airfoil. In Fig. 5a, the shock wave is steeper and decelerates flow to a subsonic speed. In

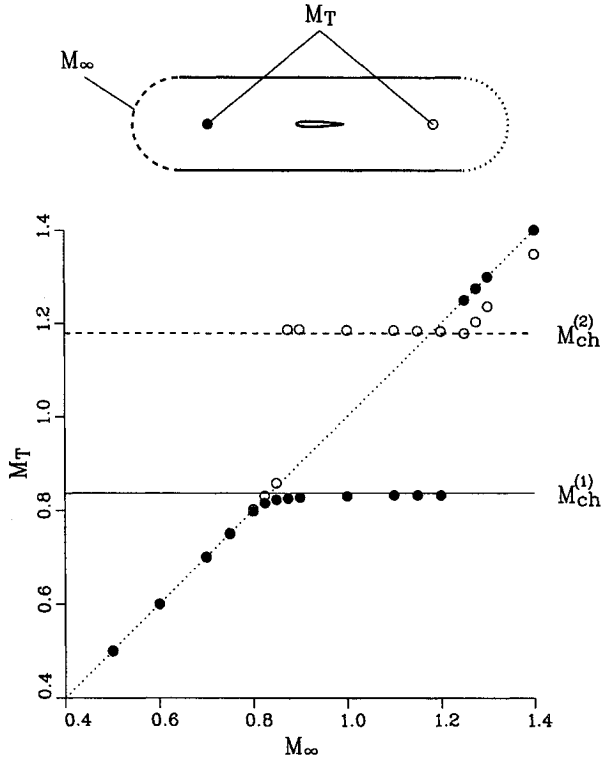

Fig. 8 Upstream and downstream Mach number as a function of Mach number at outer boundary; for a NACA 0012 in wind tunnel (h/c = 5).

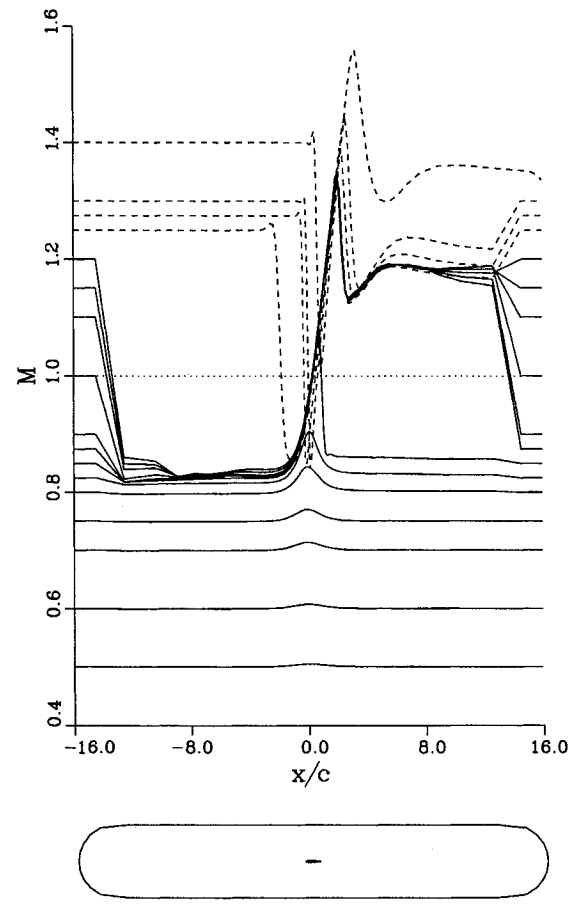

Fig. 9 Wall Mach number for a NACA 0012 in wind tunnel (h/c = 5).

Fig. 5b, the shock wave is more oblique and flow remains supersonic aft of it. Choked wind-tunnel flows of both types were observed experimentally by Collins and Krupp,[12] who also showed that the extent of the rear supersonic expansion depends on back pressure. By using an extrapolation boundary condition at the rear end of the computational domain, we had no direct control over that. The computed results were either of the type shown in Figs. 5a or 5b. The parameter determining which type of flow would be produced was not back pressure, but M_∞, specified upstream and retrieved downstream of the computational domain.

The choked-flow pattern $M_{ch}^{(2)} \rightarrow M_{ch}^{(2)}$ is shown in Fig. 5c. The upstream portion of wind-tunnel flow is supersonic and there is a detached shock wave ahead of the airfoil. Note that downstream of the dashed sonic line the isomachs in Figs. 5b and 5c are the same. The last remaining choked flow, $M_{ch}^{(2)} \rightarrow M_{ch}^{(1)}$, has not been observed. However, based on the preceding discussion, it is not difficult to imagine how this hypothetical flow pattern would appear: upstream of the dashed sonic line like that of Fig. 5c and downstream like that of Fig. 5a.

Figure 10 shows the isomachs for the free-air flow at sonic conditions, which in conjunction with Fig. 5 can be used to examine two seemingly contradicting theories. Based on a purely physical argument, Allen and Vincenti[8] argued that a steady-state flow similar to that observed in the wind tunnel at choking cannot exist in free-air. In contrast, Guderley[13] and Spreiter et al.[14] reasoned that the flow in the vicinity of the model under choking conditions bears a close resemblance to an unbounded flow with stream Mach number unity, provided the dimensions of the model are small compared with those of the test section. A resemblance of the sonic flow in Fig. 10 and choked flow $M_{ch}^{(1)} \rightarrow M_{ch}^{(2)}$ in Fig. 5b is undeniable. In both cases the supersonic expansion on the airfoil is terminated by a tail shock wave, aft of which the flow is locally supersonic. However, small differences show up almost everywhere, most notably in the shapes of sonic lines and tail shock waves. The sonic line turns in the direction normal to the test section wall, whereas in free-air its curvature decreases with distance from the airfoil. The tail shock wave in the wind tunnel is not quite as steep as that in free-air.

Correspondingly, there are also some differences in airfoil surface Mach number distributions. In Fig. 11, the choking distribution is plotted by a solid line and the distribution corresponding to the sonic flow by a broken line. Evidently, the blockage ratio $c/h = 0.2$ selected in our example was not small enough to provide an adequate agreement. Since the surface Mach distribution is invariant at $M_\infty = 1$, a very substantial reduction in M_∞ is required to reduce the distribution in free-air to that in choked flow. Our computations show that by lowering the free-air Mach number to $M_\infty = 0.85$, a very satisfactory agreement is obtained, but only over the frontal part of the airfoil. The dotted curve in Fig. 11 indicates that the tail shock has already moved forward.

The validity of the sonic-freeze principle or the stabilization law[15] with regard to both free-air and wind-tunnel flow can also be verified in Fig. 6. From the isentropic relationship

$$C_p = \frac{2}{\gamma M_\infty^2}\left\{\left[\frac{2 + (\gamma - 1)M_\infty^2}{2 + (\gamma - 1)M^2}\right]^{\gamma/(\gamma-1)} - 1\right\} \tag{3}$$

and the sonic-freeze assumption

$$\left(\frac{\partial M}{\partial M_\infty}\right)_{M_\infty=1} = 0$$

we obtain[16]

$$\left(\frac{\partial C_p}{\partial M_\infty}\right)_{M_\infty=1} = \frac{4}{\gamma + 1}\left[1 - \frac{1}{2}(C_p)_{M_\infty=1}\right] \tag{4}$$

Substituting Eq. (4) into the differentiated Eq. (2) it also follows[17]:

$$\left(\frac{\partial C_L^u}{\partial M_\infty}\right)_{M_\infty=1} = -\frac{4}{\gamma + 1}\left[1 + \frac{1}{2}(C_L^u)_{M_\infty=1}\right] \tag{5}$$

The slopes of the C_L^u-curves at $M_\infty = 1$, observed in Fig. 6, are very nearly the same and in agreement with those predicted from Eq. (5): -2.03 in free-air and in -1.98 wind tunnel. The principal difference is that the airfoil surface distribution of M in the wind tunnel is invariant on the entire choking interval $M_{ch}^{(1)} \leqq M_\infty \leqq M_{ch}^{(2)}$, whereas in free-air only on the natural, much narrower interval around $M_\infty = 1$.

A possible way to quantify the Guderley–Spreiter hypothesis is then to assume that choked flow past an airfoil is equivalent to sonic flow past the same airfoil, provided that the

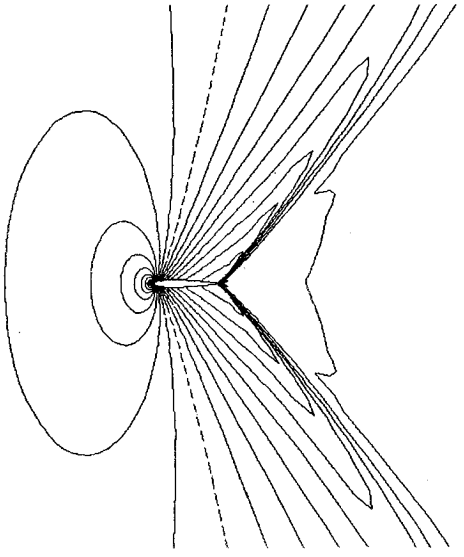

Fig. 10 Isomachs for sonic flow around a NACA 0012.

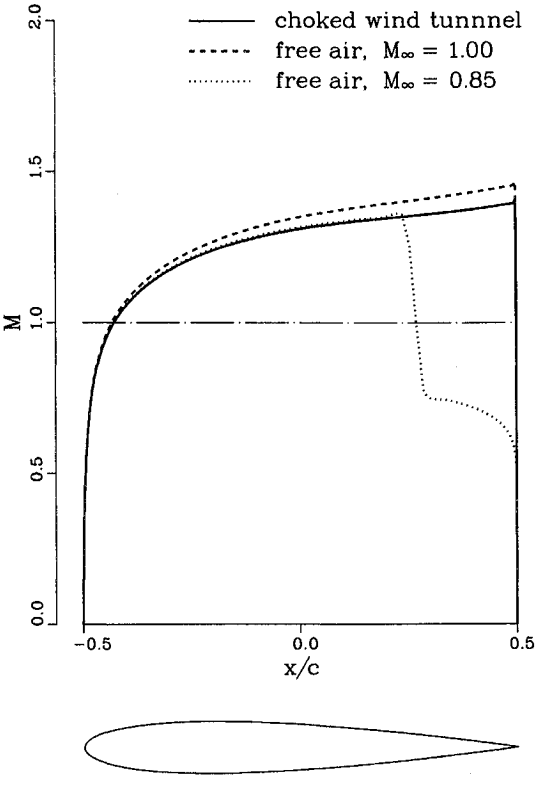

Fig. 11 Surface Mach number for a NACA 0012.

choking interval is only as wide as the natural sonic-freeze interval. However, concerning the practical applicability of the hypothesis, the results are not particularly encouraging. For example, if we are willing to accept $0.98 \leq M_\infty \leq 1.02$ as the sonic-freeze interval, then from Eq. (1) $t/h = 0.0003$, which for $t/c = 0.12$ gives $c/h = 0.0025$. The test section height would have to be 400 times the chord length of a NACA 0012. If, in the absence of rigorous quantitative criteria, we relax the sonic-freeze interval to $0.95 \leq M_\infty \leq 1.05$, a similar calculation shows that the height would have to be only about 50 chord lengths.

Referring back to Fig. 6, we would also like to make the following comment. The observed dependences of C_L^u on M_∞ are real, except for choked flow. In the latter case M_∞ is merely an artificial reference. Over the choking interval, where the surface Mach number (solid line in Fig. 11) is invariant, the local pressure coefficient is only a function of M_∞. The wind-tunnel values of C_L^u that could have been easily obtained from the choked distribution of M and Eqs. (2) and (3), without additionally running the CFD code, are plotted as crosses in Fig. 6.

As may further be established from Fig. 6 with regard to wall interference, the interval $M_\infty > M_{ch}^{(2)}$ can be divided into two subintervals: below $M_\infty \approx 1.3$, where substantial differences between the values of C_L^u computed in free-air and wind tunnels exist, and above $M_\infty \approx 1.3$, where these differences vanish. The interval, on which the wind-tunnel and free-air data differ is generally considered as uncorrectable to free-air conditions. Our numerical results (not published here) essentially support this notion. Although for a thick airfoil the interference is not necessarily as acute as that predicted for a thin airfoil by planar wave reflections,[14] the qualitative differences of observed flow patterns (e.g., the shapes and locations of the detached shock waves) are too profound to permit a meaningful correlation. When $M_\infty > 1.3$, the detached shock wave becomes more oblique and its reflected part no longer impinges on the airfoil. The airfoil data become interference free and we are finally out of the realm of transonic wall interference.

One last thing that we would like to bring up is the effect of airfoil thickness. Figure 12 shows the wind-tunnel and free-air values of C_L^u, calculated for a NACA 0006, which is half the thickness of NACA 0012. The computations were again performed for the wind-tunnel height-to-airfoil chord ratio of 5 and zero incidence. The choking interval is narrower: the one-dimensional estimates from Eq. (1) are $M_{ch}^{(1)} = 0.884$ and $M_{ch}^{(2)} = 1.124$. The values of C_L^u at $M_\infty = 1$ are 66% of those for the NACA 0012, both in free-air and the wind tunnel. The slopes of the C_L^u-curves at $M_\infty = 1$, evaluated from Eq. (5) are 94% of those for the NACA 0012. Besides these quantitative differences, a very similar wall-interference pattern is observed.

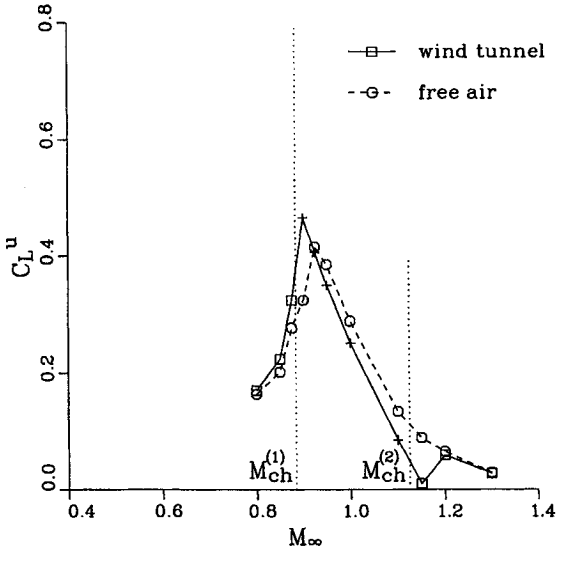

Fig. 12 Upper-surface lift coefficient for a NACA 0006 in free-air and wind tunnel ($h/c = 5$).

VI. Concluding Remarks

Numerical simulation of transonic flow past a symmetrical airfoil in a closed-wall wind tunnel has been conducted. Among the important conclusions to be drawn from this study are that for airfoils of finite thickness, transonic wall interference is not restricted to a narrow interval around Mach unity, but rather to wider intervals of stream Mach number adjacent to the choking interval. By tuning the Mach number at the upstream end of the computational domain, three different, physically meaningful choked-flow solutions were produced. The Guderley–Spreiter hypothesis, according to which there is an equivalence of the choked flow and free-air flow at sonic conditions, has been re-examined. By comparing the intervals of choked flow and naturally frozen free-air flow, it is demonstrated that an adequate correspondence can be established only for extremely large wind-tunnel height-to-airfoil chord ratios (50 or more).

An extension of the present analysis to a lifting airfoil would be of interest for two reasons: choking does not occur on the upper and lower surfaces simultaneously and wall interference is a two-parameter problem, involving the corrections to Mach number and angle of attack. Using the approach described in this article, no problems were found in running the NPARC code for a wind-tunnel flow past a NACA 0012 at incidence. However, a suitable strategy has yet to be devised to present the data and minimize, accordingly, the number of required computations.

The NPARC code has proven to be an excellent flow simulation tool in this specific application-oriented environment.

Acknowledgments

This study was performed under project Wind Tunnel Wall Interference of the Institute of Aerospace Research, National Research Council of Canada. The authors would like to thank the Arnold Engineering and Development Center/NASA for providing the NPARC code. Special thanks go to Y. Y. Chan of the Institute of Aerospace Research for helpful suggestions and calling attention to some important references. The second author also gratefully acknowledges a discussion of the preliminary results with R. Dvorak of the Czech Academy of Sciences and K. Kozel of the Technical University of Prague.

References

[1]Goodman, T. R., "A Criterion for Assessing Wind-Tunnel Wall Interference at Mach 1," *Journal of Aircraft*, Vol. 10, No. 11, 1973, pp. 695–697.

[2]Cole, J. D., Malmuth, N. D., and Zeigler, F., "An Asymptotic Theory of Solid Tunnel Wall Interference on Transonic Airfoils," AIAA Paper 82-0933, June 1982.

[3]Cole, J. D., and Cook, L. P., "Two-Dimensional Choked Transonic Flow," *Journal of Applied Mathematics and Physics (ZAMP)*, Vol. 39, Jan. 1988, pp. 1–12.

[4]Cook, L. P., "Some Problems in Transonic Aerodynamics," AIAA Paper 95-0476, Jan. 1995.

[5]Cooper, G. K., and Sirbaugh, J. R., "PARC Code: Theory and Usage," Arnold Engineering and Development Center TR-89-15, Dec. 1989.

[6]Kraft, E. M., Ritter, A., and Laster, M. L., "Advances at AEDC in Treating Transonic Wind Tunnel Wall Interference," *Proceedings of the 15th Congress of the International Council of the Aeronautical Sciences*, Vol. 2, 1986, pp. 748–769.

[7]Hawken, D. F., "A TVD Multigrid Multiblock Euler Code Applied to Wind-Tunnel Corrections," *Proceedings of the 2nd Annual Conference of the CFD Society of Canada* (Toronto, Canada), 1994, pp. 27–34.

[8]Allen, H. J., and Vincenti, W. G., "Wall Interference in a Two-

Dimensional-Flow Wind Tunnel, with Consideration of the Effect of Compressibility," NACA 782, 1944.

[9]Green, L. L., and Newman, P. A., "Wall-Interference Assessment and Corrections for Transonic NACA 0012 Airfoil Data from Various Wind Tunnels," NASA TP-3070, April 1991.

[10]Ferri, A., *Elements of Aerodynamics of Supersonic Flows*, Macmillan, New York, 1949, pp. 181–188.

[11]Mokry, M., "On the Subsonic and Transonic Doublet in the Far-Field Representation of an Airfoil," AIAA Paper 95-1879, June 1995.

[12]Collins, D. J., and Krupp, J. A., "Experimental and Theoretical Investigations in Two-Dimensional Transonic Flow," *AIAA Journal*, Vol. 12, No. 6, 1974, pp. 771–778.

[13]Guderley, K. G., *The Theory of Transonic Flow*, Pergamon, 1962, pp. 274–280.

[14]Spreiter, J. R., Smith, D. W., and Hyett, B. J., "A Study of the Simulation of Flow with Free-Stream Mach Number 1 in a Choked Wind Tunnel," NASA TR R-73, Jan. 1960, pp. 771–778.

[15]Cook, L. P., and Zeigler, F. J., "The Stabilization Law for Transonic Flow," *SIAM Journal on Applied Mathematics*, Vol. 46, No. 1, 1986, pp. 27–48.

[16]Liepmann, H. W., and Roshko, A., *Elements of Gasdynamics*, Wiley, New York, 1957, pp. 274, 275.

[17]Dvorak, R., *Transonic Flow*, Academia, Prague, 1986, pp. 131, 132 (in Czech).